Non-isochronism and energy dynamics of an interrupted pendulum

M. Salman Hassan[a], **Huzaifa Shehzad Amin**[a], **Annia Bilal Malik**[a], **and Hibah Faisal**[a]

[a]Physlab, Lahore University of Management Sciences

This experiment investigated the period-amplitude relationship of an interrupted pendulum for various horizontal peg offsets ($z = +20, +10, 0, -10, -20$ cm). Our results confirm the theoretical predictions of Gil and Di Gregorio: when the peg is displaced horizontally from the vertical line of suspension ($z \neq 0$), the period does not converge to a single value as amplitude decreases. The symmetric case ($z = 0$) exhibits near-isochronous behavior with minimal period variation. Video analysis reveals exponential energy decay with damping coefficients $\lambda = 0.016-0.026$ s^{-1}, varying with peg position.

Interrupted Pendulum | Non-isochronism | Harmonic Motion | Damping

The interrupted pendulum consists of a simple pendulum whose string contacts a rigid peg during oscillation, changing its length mid-swing. Unlike a simple pendulum that becomes isochronous for small amplitudes, the interrupted pendulum has non-isochronous behavior when the peg is displaced horizontally in the vertical axis.

Gil and Di Gregorio [1] demonstrated both theoretically and experimentally that when the peg offset $z \neq 0$, the period diverges as amplitude approaches zero, with different offsets producing distinct limiting periods. This arises because the system behaves as two harmonic oscillators with different natural frequencies.

We set up experimental apparatus to test these predictions across five peg positions, measuring period-amplitude relationships via stopwatch timing and motion dynamics via video tracking using the Tracker software [2].

1. Theory

The pendulum has full suspension length $l_0 = 84.9$ cm. The peg is positioned at vertical distance y_0 below the suspension point and horizontal distance z from the vertical axis (positive when displaced to the right) as shown in Figure 1.

According to Gil and Di Gregorio [1], for small angular amplitudes where $\sin\theta \approx \theta$, the period is given by:

$$T_{12} = \frac{1}{2}(T1 + T2) = \pi\left(\sqrt{\frac{l_0}{g}} + \sqrt{\frac{l_0 - y_0}{g}}\right) \qquad [1]$$

where θ_0 is the maximum angular amplitude and g is gravitational acceleration. The critical prediction is the $1/\theta_0$ term for $z \neq 0$: as amplitude approaches zero, the period does not converge to a single value but instead approaches a limit [1].

The non-isochronism arises from the piecewise parabolic potential structure. For $z \neq 0$, the interrupted pendulum experiences a potential consisting of two parabolas with different curvatures, joined at angular position $\theta = \alpha = z/y_0$ [1]. Oscillations of different amplitudes experience different restoring force constants. This anharmonicity can be detected through Fourier analysis, where higher harmonics become increasingly important as amplitude increases [4].

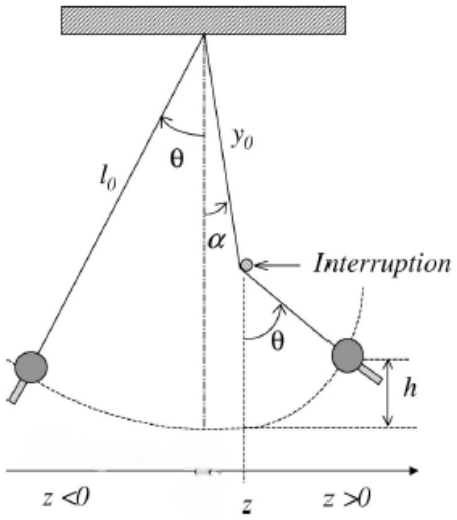

Fig. 1. Schematic diagram of the interrupted pendulum geometry showing full suspension length l_0, peg vertical position y_0 from suspension point, and horizontal offset z from vertical axis. (adapted from Gil & Di Gregorio [1])

In the presence of air resistance and friction, the system shows light damping. For underdamped oscillations, total mechanical energy decays exponentially:

$$E(t) = E_0 e^{-\lambda t} \qquad [2]$$

where λ is the damping coefficient and E_0 is the initial energy.

2. Methods

Apparatus. The apparatus consisted of a pendulum bob of mass $m = 0.046$ kg suspended by an inextensible string of length $l_0 = (84.9 \pm 0.2)$ cm. The peg assembly included a rigid cylindrical peg mounted on a board allowing adjustment of horizontal offset z. Motion was captured using a 120 fps video camera. Measurement tools included a protractor for initial angle setting and a meter stick for length measurement.

Procedure. Five horizontal offsets were tested: $z = +20, +10, 0, -10, -20$ cm. For each configuration, the peg vertical position y_0 was measured. Table 1 summarizes the parameters.

For each peg configuration and initial amplitude $\theta_0 = 0.10-0.40$ rad, we timed 10 complete oscillations three times using a digital stopwatch. The period was calculated as $T = t_{\text{avg}}/10$. Motion was also recorded at 120 fps and analyzed frame-by-frame using Tracker software [2] to extract angular position $\theta(t)$ and angular velocity $\dot{\theta}(t)$, as well as kinetic energy

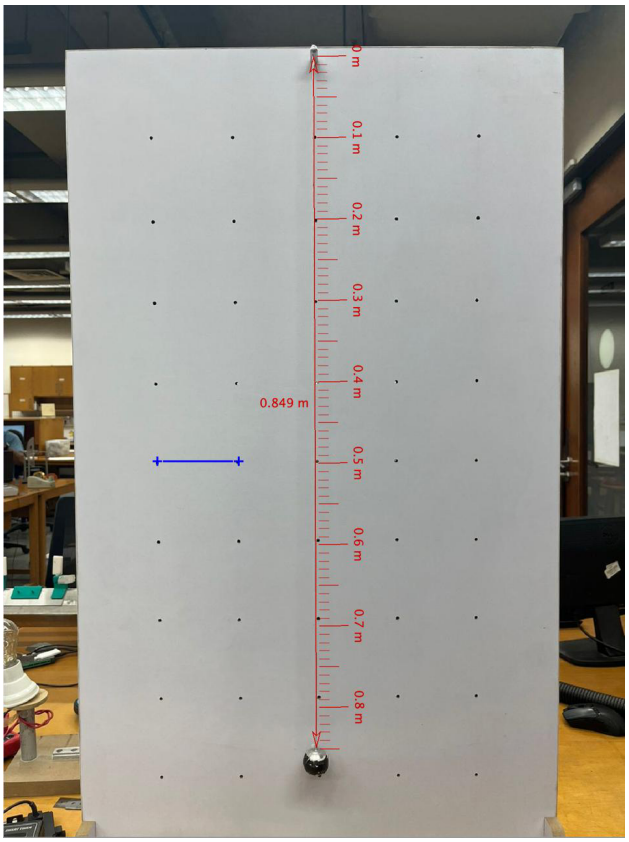

Fig. 2. Photograph of the experimental apparatus showing the pendulum bob, adjustable horizontal peg rail, and high-speed camera positioned for motion tracking. A scale factor of 10cm was measured (blue line).

Table 1. Measured parameters

z (cm)	y_0 (cm)
$+20$	72.5
$+10$	70.3
0	69.6
-10	70.3
-20	72.5

K, potential energy U, and total energy $E = K + U$ for energy decay analysis.

3. Results

Tables 2 through 6 present the raw period measurements for all configurations. For each amplitude, three timing trials were performed and averaged.

Table 2. Period measurements for $z = 0$ cm

θ (rad)	t_1 (s)	t_2 (s)	t_3 (s)	t_{avg} (s)	T (s)
0.10	12.38	12.51	12.43	12.44	1.244
0.15	12.68	12.55	12.66	12.63	1.263
0.20	13.22	13.34	13.34	13.30	1.330
0.25	13.21	13.34	13.29	13.28	1.328
0.30	13.47	13.35	13.41	13.41	1.341
0.35	13.38	13.52	13.45	13.45	1.345
0.40	13.62	13.51	13.58	13.57	1.357

4. Analysis and Discussion

Figure 3 presents the measured periods overlayed with theoretical curves calculated from Eq. 1. There is good agreement

Table 3. Period measurements for $z = +10$ cm

θ (rad)	t_1 (s)	t_2 (s)	t_3 (s)	t_{avg} (s)	T (s)
0.20	16.98	17.15	17.05	17.06	1.706
0.25	16.52	16.40	16.49	16.47	1.647
0.30	16.38	16.29	16.41	16.36	1.636
0.35	15.42	15.55	15.44	15.47	1.547
0.40	15.12	15.24	15.21	15.19	1.519

Table 4. Period measurements for $z = +20$ cm

θ (rad)	t_1 (s)	t_2 (s)	t_3 (s)	t_{avg} (s)	T (s)
0.30	18.04	18.21	18.11	18.12	1.812
0.35	17.34	17.48	17.38	17.40	1.740
0.40	17.26	17.12	17.19	17.19	1.719

Table 5. Period measurements for $z = -10$ cm

θ (rad)	t_1 (s)	t_2 (s)	t_3 (s)	t_{avg} (s)	T (s)
0.20	9.39	9.28	9.35	9.34	0.934
0.25	10.42	10.51	10.48	10.47	1.047
0.30	11.12	11.36	11.24	11.24	1.124
0.35	11.43	11.58	11.49	11.50	1.150
0.40	11.89	11.78	11.94	11.87	1.187

Table 6. Period measurements for $z = -20$ cm

θ (rad)	t_1 (s)	t_2 (s)	t_3 (s)	t_{avg} (s)	T (s)
0.30	8.15	8.02	8.10	8.09	0.809
0.35	9.31	9.19	9.25	9.25	0.925
0.40	9.82	9.65	9.75	9.74	0.974

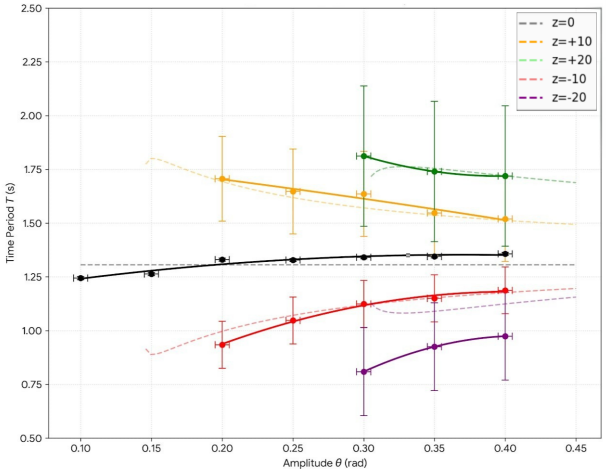

Fig. 3. Experimental period vs amplitude (data points with error bars) overlayed with theoretical predictions (dashed curves). Each color represents a different peg offset z. The divergence at small amplitudes for $z \neq 0$ confirms the non-convergence prediction.

across all configurations. For $z \neq 0$, as θ_0 decreases, periods approach distinct values: $T \to 1.8$ s for $z = +20$ cm, $T \to 1.6$ s for $z = +10$ cm, $T \to 1.0$ s for $z = -10$ cm, and $T \to 0.8$ s for $z = -20$ cm. The symmetric case $z = 0$ shows minimal period variation, exhibiting near-isochronous behavior.

Figure 4 presents angular position versus time for all configurations. The oscillation frequency varies systematically with peg offset: negative z values complete significantly more cycles in equivalent time intervals than positive z values. The amplitude decreases due to damping. The $z = 0$ configuration has the most regular and symmetric pattern.

Fast Fourier Transform (FFT) analysis independently verified our stopwatch measurements. Figure 5 presents amplitude

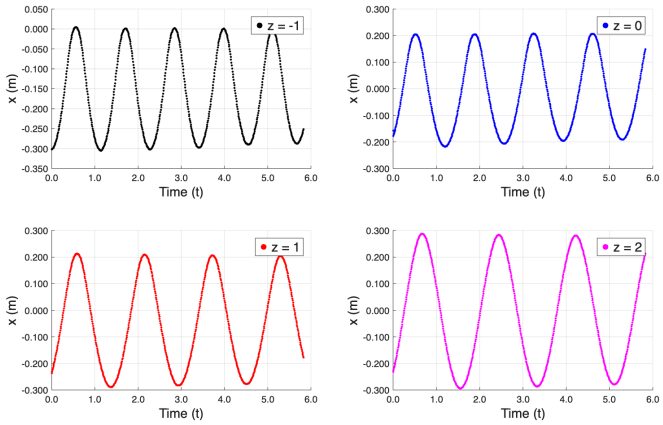

Fig. 4. Angular position versus time for all peg configurations: (a) $z = -20$ cm, (b) $z = -10$ cm, (c) $z = 0$ cm showing symmetric pattern, (d) $z = +10$ cm, (e) $z = +20$ cm. The oscillation frequency varies systematically with peg offset, with negative z values completing more cycles in equivalent time intervals. All configurations exhibit amplitude decay due to damping.

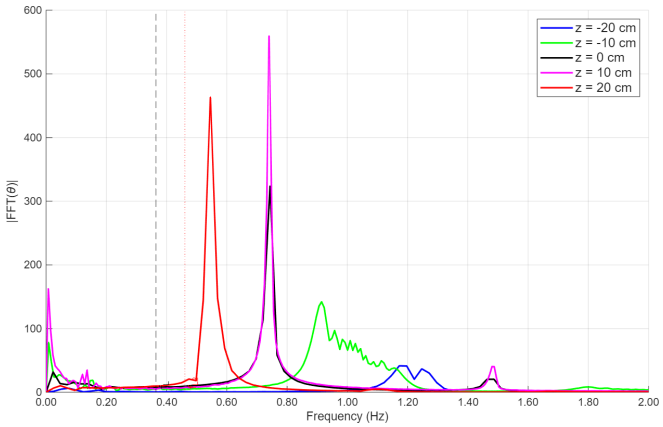

Fig. 5. FFT amplitude spectra for all five peg configurations. Each curve exhibits a dominant peak at its characteristic frequency $f = 1/T$. Peak positions shift systematically with z.

spectra for all configurations. The peaks identify the dominant oscillation frequency. Fundamental frequencies extracted from FFT agree with stopwatch measurements of time period (calculated using $f = 1/T$).

Figure 6 illustrates energy dynamics for the $z = 10$ cm configuration. When kinetic energy is at its maximum, potential energy is at its minimum, and vice versa. Total mechanical energy decreases exponentially due to light damping.

The potential energy diagram (Figure 7) provides comparison of all offset values. When the offset is non-zero ($z \neq 0$), the interrupted pendulum exhibits a composite potential composed of two parabolas with different curvatures, joined at a point displaced from the system's geometric center. Oscillations with different amplitudes sample different portions of this asymmetric potential. This results in the pendulum experiencing different restoring force constants, causing amplitude-dependent periods [1].

Figure 8 presents the fit of the experimental potential energy data for the centered configuration ($z = 0$) against the theoretical potential energy equation [1].

The general theoretical potential energy $V(\theta)$ for the interrupted pendulum is given by:

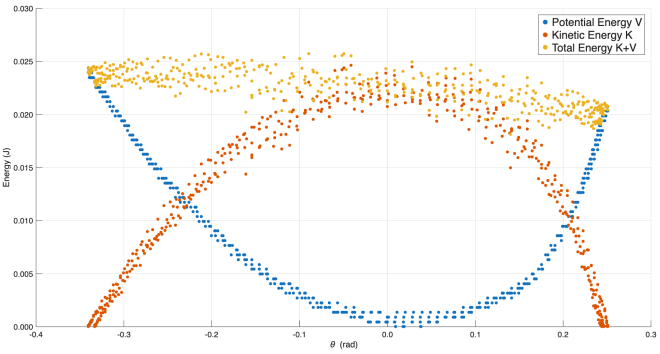

Fig. 6. Kinetic, potential, and total mechanical energy versus time for $z = 10$ cm. The energies oscillate in antiphase, while total energy exhibits smooth decay.

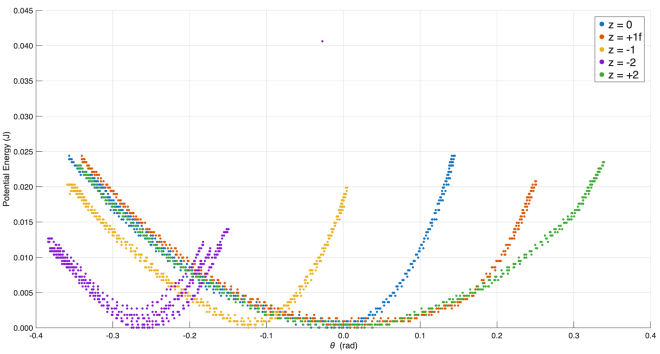

Fig. 7. Theoretical effective potential energy showing piecewise parabolic structure. For $z \neq 0$, the two segments have different curvatures. (From Gil & Di Gregorio [1])

$$V(\theta) = \begin{cases} \frac{1}{2}\mathcal{I}\omega_1^2\theta^2, & \text{if } \theta \leq \alpha, \\ \frac{1}{2}\mathcal{I}\omega_1^2 \left(\frac{l_0 - y_0}{l_0}\right)\left(\theta^2 + \left(\frac{y_0}{l_0 - y_0}\right)\alpha^2\right), & \text{if } \theta > \alpha, \end{cases}$$

Since the offset z is proportional to y_0, the centered configuration ($z = 0$, meaning $y_0 = 0$) causes the general two-part potential to reduce to the top case ($V(\theta) = \frac{1}{2}\mathcal{I}\omega_1^2\theta^2$) for all $\theta \leq \alpha$, effectively creating a smooth, single-well, symmetric parabola. The agreement between the experimental data points and the theoretical parabolic curve, confirms this $\mathbf{z = 0}$ configuration acts as a simple harmonic oscillator and is responsible for observed near-isochronous behavior [1].

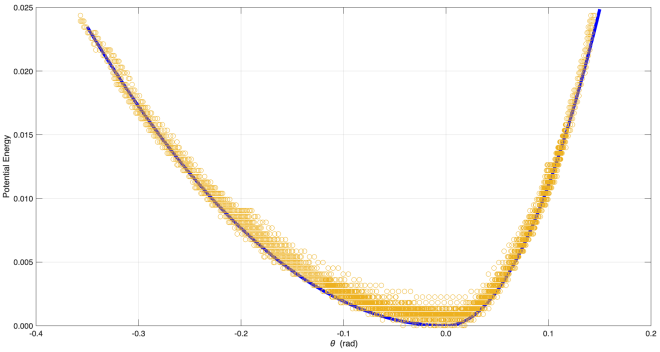

Fig. 8. Experimental potential energy data (points) for $z = 0$ cm with theoretical parabolic fit (curve). The agreement demonstrates a smooth, single-well potential.

For damping analysis, we plotted $\ln(E_{\max})$ versus time. According to Eq. 2, exponential decay appears linear on a log-

arithmic scale with slope $-\lambda$ (damping co-efficient). Figure 9 confirms this relationship. Damping coefficient uncertainties were calculated from the standard error of the linear regression slope, yielding typical uncertainties of approximately ± 0.002 s^{-1}. Linear regression yielded the damping coefficients in Table 7.

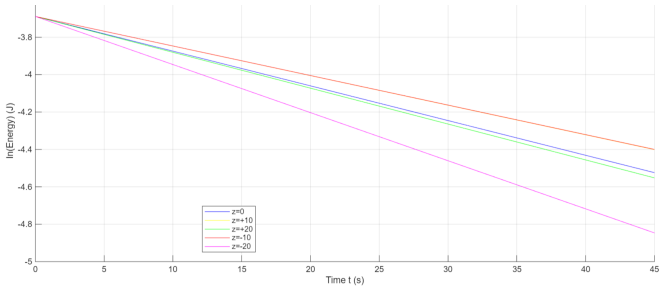

Fig. 9. Natural logarithm of peak total energy versus time for all configurations. Linear relationships confirm exponential decay. Steeper slopes for larger z indicate more damping.

Table 7. Damping coefficients from energy decay fits

z (cm)	λ (s^{-1})
$+20$	0.019 ± 0.002
$+10$	0.016 ± 0.002
0	0.019 ± 0.001
-10	0.016 ± 0.002
-20	0.026 ± 0.002

The damping coefficient λ ranges from 0.016 ± 0.002 to 0.026 ± 0.002 s^{-1}. The highest damping occurs at $z = -20$ cm ($\lambda = 0.026 \pm 0.002$ s^{-1}), while the lowest occurs at $z = -10$ cm and $z = +10$ cm ($\lambda = 0.016 \pm 0.002$ s^{-1}). The variation suggests the string-peg interaction introduces additional dissipation for reasons other than air resistance, likely from friction at the contact point or string tension fluctuations.

5. Uncertainty Analysis

Type A and Type B uncertainties were combined to determine total measurement uncertainty. Type A uncertainty from the standard deviation of three timing trials showed stark differences: at $z = 0$, consistent isochronous behavior yielded $\sigma_T \approx 0.0070$ s, while at $z = 20$ cm, the continuously shifting period during amplitude decay increased uncertainty to $\sigma_T \approx 0.33$ s.

Type B uncertainty included human reaction time (± 0.1 s per measurement, giving $\delta T_{\text{reaction}} = 0.010$ s for 10 oscillations). Total period uncertainty was $\delta T_{\text{total}} = \sqrt{\delta T_{\text{reaction}}^2 + \sigma_T^2}$.

For damping coefficient uncertainty, linear regression of $\ln(E_{max})$ vs t yields standard error of the slope $\Delta\lambda$, with uncertainties of 0.001-0.002 s.

6. Conclusion

This experiment successfully verified the non-isochronous behavior of the interrupted pendulum as predicted by Gil and Di Gregorio [1]. For all $z \neq 0$ configurations, the period fails to converge as amplitude decreases, instead approaching z-dependent limits ranging from 0.8 s to 1.8 s. The symmetric case $z = 0$ shows less variation, demonstrating that only symmetric interruption preserves some isochronous behavior.

Experimental data match theoretical predictions for amplitude v. time graphs. Video analysis revealed asymmetric oscillation dynamics predicted by the piecewise parabolic potential model. Energy analysis characterized light exponential decay with $\lambda = 0.016{-}0.026$ s^{-1}.

This experiment demonstrates that horizontal displacement of the interruption point alters oscillatory behavior.

References

[1] S. Gil and D. E. Di Gregorio, "Nonisochronism in the interrupted pendulum," *American Journal of Physics* **71**(11), 1115–1120 (2003).

[2] D. Brown, "Tracker Video Analysis and Modeling Tool," https://physlets.org/tracker/ (accessed November 2025).

[3] M. Giliberti et al., "Detecting anharmonicity at a glance," *European Journal of Physics* **35**, 065012 (2014).

[4] S. Gil, A. E. Legarreta, and D. E. Di Gregorio, "Measuring anharmonicity in a large amplitude pendulum," *American Journal of Physics* **76**(9), 843–847 (2008).